Electronic Supplementary Information

Assembled growth of 3D Fe_3O_4@Au nanoparticles for efficient photothermal ablation and SERS detection of microorganisms

Wei-En Hong,[†a] I-Ling Hsu,[†a] Szu-Yung Huang,[†a] Chien-Wei Lee,[†a] Han Ko,[a] Pei-Jane Tsai,[b] Dar-Bin Shieh,[c,d] and Chih-Chia Huang[*a,d]

a. Department of Photonics, National Cheng Kung University, Tainan, Taiwan
Email: c2huang@email.ncku.edu.tw

b. Department of Medical Laboratory Science and Biotechnology, College of Medicine, National Cheng Kung University, Tainan, Taiwan

c. Institute of Oral Medicine and Department of Stomatology, College of Medicine, National Cheng Kung University and Hospital, Tainan, Taiwan

d. Center of Applied Nanomedicine and Center for Micro/Nano Science and Technology, National Cheng Kung University, Tainan, Taiwan

† These authors contribute equally to this work.

Supplementary experimental details

Chemicals. Hydrogen tetrachloroaurate(III) trihydrate ($HAuCl_4 \cdot 3H_2O$), hydrazine monohydrate (N_2H_4), 3,4-dihydroxy-L-phenylalaine (L-dopa), 4-ATP, MB and iron(II,III) oxide Fe_3O_4 were purchased from Alfa Aesar. Ferrous chloride tetrahydrate ($FeCl_2 \cdot 4H_2O$) and sodium citrate dihydrate were obtained from J. T. Baker. 1,3,5-Benzenetricarboxylic acid (TMA) and 4-nitrophenol (4-NTP) were purchased from ACROS. 3,3',5,5'-Tetramethylbenzidine (TMB) and iron(III) oxide (γ-Fe_2O_3) nanopowder were obtained from Sigma-Aldrich. Magnetic Fluid-Carboxyl was purchased from MagQu. Luria-Bertani (LB) broth (Miller) was purchased from AthenaES. Agar was purchased from Amresco. BacTiter-Glo Microbial Cell Viability Assay was obtained from Promega. Phosphate buffered saline (PBS) was obtained from Thermo.

Preparation of the NIR-activated Fe_3O_4 nanoparticles. The Fe_3O_4 nanoparticle clusters were prepared by a hydrothermal reaction of 4.5 ml of trimesic acid (25 mM), 150 mg of sodium citrate, 10 ml of $FeCl_2$ (50 mM) and 0.1 ml of N_2H_4 at 200 °C for 13 hours, following our previously reported synthesis process.[1] Afterwards, we employed a repeated centrifugation and washing process with deionized water to purify the as-synthesized Fe_3O_4 nanoparticles.

Preparation of the Fe_3O_4@Au nanohybrid. A $HAuCl_4$ (1.2 ml, 5 mM) solution and 2.15 ml of deionized water were mixed in a sonication bath for 1 minute, followed by adding 0.5 ml of Fe_3O_4 nanoparticles (400 ppm) prepared according to atomic absorption spectroscopy (AAS) measurements. Subsequently, 1.2 ml of L-dopamine (20 mM) was injected into the Fe_3O_4/$HAuCl_4$ solution, and the resulting mixture was heated at 80 °C for 10 minutes. Finally, a repeated process of centrifugation at 1100 rpm and washing with deionized water was employed to purify the Fe_3O_4@Au nanohybrid. Finally, the sample was collected after centrifugation at 3000 rpm and stored at 4 °C for further application.

Photothermal examination with 785 nm/808 nm/1064 nm lasers. The Fe_3O_4@Au nanohybrid (200 μL, 50 $ppm_{[Fe]}$) was added to each well of a 96-well plate and individually irradiated with 1.25

mW/cm^2 lasers with 785 nm, 808 nm, and 1064 nm wavelengths. The light was irradiated from the bottom of the plate across the sample solution. The temperature increment of the solution was recorded using a T-type thermocouple thermometer with irradiation time.

Photothermal antibacterial experiment. The Fe_3O_4@Au nanohybrid (50 $ppm_{[Fe]}$) was placed into a 96-well plate, and 100 μl of bacterial culture (2×10^5 CFU/ml) suspended in PBS was added. Subsequently, the bacteria were irradiated with an 808 nm continuous-wave laser for 10 minutes. The mixture was 100-fold diluted in PBS, and then, 100 μl of the diluted mixture was spread on an agar plate. After 24 hours of incubation at 37 °C, the viable colonies were counted.

Recyclable PTA toward bacteria. After the photothermal antibacterial experiment, the Fe_3O_4@Au nanohybrid was collected using a magnet, washed twice with deionized water and resuspended in PBS. Subsequently, the collected Fe_3O_4@Au nanohybrid was subjected to another photothermal antibacterial experiment.

Photothermal effect on cell viability. Mouse embryonic fibroblast NIH/3T3 cells were seeded at a density of 8000 cells/well in 96-well plates and incubated for 24 h. To measure the cytotoxicity of the Fe_3O_4@Au nanohybrids, the cells were treated with Fe_3O_4@Au nanohybrids for 24 h. To measure the Fe_3O_4@Au nanohybrid-mediated photothermal effect on NIH/3T3 cell viability, the cells were treated with Fe_3O_4@Au nanohybrids for 3 h, followed by removing the unbound nanoparticles and then irradiating with an 808 nm laser (1.25 W/cm^2) for 10 min. The irradiated cells were further incubated for 24 h. The cell viability was evaluated by an MTT assay.

Detection of molecules with Fe_3O_4@Au nanohybrid. To measure the SERS, 5 μl of a MB solution (10^{-3}-10^{-7} M) and 100 μl of 4-ATP (10^{-3}-10^{-10} M) were directly mixed with the Fe_3O_4@Au nanohybrid (50 $ppm_{[Fe]}$). An additional incubation of 6 h was applied for the immobilization of 4-ATP to the surface of the Fe_3O_4@Au nanohybrid. After centrifugation, the 4-ATP-coated Fe_3O_4@Au nanohybrid solution was resuspended in 100 μl of deionized water. A 10 μl solutions of the Fe_3O_4@Au/MB nanohybrid and 4-ATP-coated Fe_3O_4@Au nanohybrid were placed on

silicon substrates. The Raman spectra of all the samples were measured with a 785 nm laser (10 mW) and 10 second integration time. In addition, the magnetic-field-induced aggregates of the Fe_3O_4@Au nanohybrid were employed to evaluate their SERS effect.

SERS measurements of microorganisms. A 100 μl bacterial suspension (10^7 CFU/ml) was centrifuged at 5000 rpm for 5 minutes. After removing the supernatant, the bacterial pellet was resuspended in 5 μl solution including 4-ATP-immobilized Fe_3O_4@Au nanohybrid. The Fe_3O_4@Au particle combined sample was separated from the solution and then concentrated onto a silicon substrate with a magnet. After drying, the micro-Raman system with 100X microscope objective lens was employed to detect the region of interest for the *E. coli* O157:H7 (under 1 second).

Characterizations. Transmission electron microscopy (TEM, Hitachi H7500 TEM instrument at 80 kV) was used to determine the structures of the nanomaterials. The absorption spectra of the Fe3O4@Au nanohybrid were measured using a V-730 UV-Vis spectrophotometer from Jasco (USA). The Fe concentrations of the Fe-based materials were quantified by AAS (SensAA GBC, Australia). The particle sizes and zeta potentials (HORIBA, Ltd., Japan) of the Fe3O4@Au nanohybrid samples dispersed in aqueous solution were measured. The magnetic nanoparticles were magnetized (M-H loops) at 300 K under applied fields up to 40 kOe using a Quantum Design MPMS-7 superconducting quantum interference device (SQUID) magnetometer.

In the Raman analysis, the samples were placed onto silicon substrates using a micropipette and were subjected to micro-Raman spectroscopy equipped with a 785 nm laser (DPSSL Driver II, 10 mW) and an MRS-iHR320 modular Raman system equipped with an Olympus BX53 microscope. A 40X objective lens and a 10 second accumulation time were applied in the Raman measurements. The Raman enhancement factor (EF) of the Fe_3O_4@Au nanohybrid substance was determined using the following equation:

$$EF = (I_{SERS} / I_{free\ substrate}) \times (N_{free\ substance\ concentration} / N_{Fe3O4@Au\ nanohybrid\ substance\ concentration})$$

where I_{SERS} and $I_{free\ substrate}$ correspond to the vibrational scattering intensities in the SERS and normal Raman spectra, respectively. I_{SERS} and $I_{free\ substrate}$ were calculated for the strongest peak of the targeting substrate. $N_{free\ substance\ concentration}$ and $N_{Fe3O4@Au\ nanohybrid\ substance\ concentration}$ represent the concentration of the molecules on the surface of a Si wafer. In the EF estimation, we assumed that the molecules in a liquid drop were homogeneously distributed on the Si wafer and exposed to the incident laser beam.

Table S1. Summary comparison of the synthesis methods and the structures of Fe_3O_4/Au hybrid nanomaterials.

Shape	Synthesis method	Reaction time	Particle size	Ref
Leukocyte-like	Site-selected atom deposition process Reduction of HAuCl4 with L-dopamine,	react at 80 °C for 10 min	224±33 nm	This study
Core-shell	Thermal decomposition Reduction by 1,2-hexadecanediol	react at 120 °C for 30min heat up to 260 °C for 150 min 30 min for cooling down	14 nm	[2]
Dimers flower-like	Thermal decomposition from Au NCs, oleic acid, 1-octadecene and oleylamine (organic medium) Two different iron precursors, $Fe(CO)_5$ and $Fe(acac)_3$	react at 315 °C for 50 min heat up to 205 °C for 2 h、315 °C for 2 h	~22 nm	[3]
Dumbbell-like flower-like Core-shell	Thermal decomposition Reduction by 1,2-hexadecanediol	200 °C for 30 min (dumbbell-like), 90 min (flower-like), 180 min (core-shell)	~12 nm	[4]
Dumbbell-like	Decomposition of $Fe(CO)_5$ on the surface of the Au Oxidation in 1-octadecene solvent	react at 120 °C for 20 min heat up to 310 °C for 45 min	dAu=2-8 nm dFe_3O_4= 4-20 nm	[5]
Flower-like	One-step solvothermal method.	stir for 30 min heat up at 200 °C for 6 h	150 nm	[6]
Core-shell	Co-precipitation Reduction by citrate	the reaction mixture was boiled under stirring for 15 min.	30 nm	[7]
Core-shell	Thermal decomposition Reduction byoleylamine (organic medium)	reaction for 20 h	12 nm	[8]

Table S2. Summary comparison of Fe_3O_4/Au hybrid nanomaterial applications.

Shape	Particle Size (nm)	Application	Ref
Fe_3O_4@PZS@Au (Core@hybrid@shell)	253±20 Fe_3O_4: 8.2±1.1 Fe_3O_4@PZS: 228.5±15 Au NPs: 3	MRI and phototheral therapy	[9]
Fe_3O_4@Au (Core@shell)	30±5 Fe_3O_4:20 Au NPs: 4±1	Bioseperation (functionalized and magnetic) and SDS-PAGE analysis	[10]
γFe_2O_3@Au (Nanoflowers)	179 Fe_3O_4: 5	Cancer theranostics (PTT+MR/PA/SERS)	[11]
Fe_3O_4@Au (Nanoeggs)	NA	PTT (Selective killing of antibiotic-resistant bacteria)	[12]
Fe_3O_4@Au@Ag (Nanoflowers)	NA	SERS monitoring of catalytic reactions	[13]
Fe_3O_4@Au@PEI (Core@shell)	300+3~5 Fe_3O_4: 300 Au NPs: 3~5	Label-free bacteria SERS detection	[14]

Table S3. Comparison summary of nanoparticle-based antibacterial treatment by using PAT processes.

Antibacterial activity against	Type of gold nanoparticles	Size (nm)	Concentration	Irradiation (W/cm^2)	Times (sec)	Wavelength (nm)	Additional surface modification/ drug loading	No of killed bacteria	Ref
Escherichia coli	Leukocyte-like Fe_3O_4@Au	254	0.76 mg/ml (50 ppm $_{[Fe]}$)	1.25	600	808	No	$2 \times 10^{4*}$	this work
	Gold nanorod/hollow SiO2 nanocapsule	205	8.58 mg/ml	0.12	1200	785	Kanamycin-loading	500	[15]
	Polygonal gold nanoparticle	70-120	83 mg/ml	0.200	300	808	Vancomycin-loading	2.5×10^4	[16]
	Spherical graphene oxide	5-8	0.8 mg/ml	1.25	600	808	Glutaraldehyde	2×10^5	[17]
Staphylococcus aureus	Leukocyte-like Fe_3O_4@Au	254	0.76 mg/ml (50 ppm $_{[Fe]}$)	1.25	600	808	No	2×10^4	this work
	Spherical graphene oxide	5-8	0.8 mg/ml	1.25	600	808	Glutaraldehyde	2×10^5	[17]
	Spherical gold nanoparticle	42	0.05 mg/ml	2	600	808	IgG antibody	100	[18]
	SiO_2 nanoparticle	73	5.45 mg/ml	1.5	300	808	poly(allylamine) and vancomycin-modified polyelectrolyte-cypate complexes	1×10^7	[19]

*Notes: *E. coli* O157:H7 and extended-spectrum beta-lactamases resistant (ESBL) *E coli* were used in our antibacterial assay. Bacterial viability is measured using minimum biocidal concentration (MBC) method.

Table S4. Comparison summary of nanoparticle-based antibacterial treatment to anaerobic and facultative anaerobic bacteria by using PAT processes.

Antibacterial activity against*	Type of gold nanoparticles	Size (nm)	Concentration (mg/mL)	Irradiation energy	Times (sec)	Wavelength (nm)	Additional surface modification/ drug loading	No of killed bacteria	Ref
Porphyromonas gingivalis	Leukocyte-like Fe_3O_4@Au	254	0.76 mg/ml (50 ppm $_{[Fe]}$)	1.25 W/cm^2	600	808	No	2×10^4	this work
Corynebacterium pseudotuberculosis	Spherical gold nanoparticle	25	0.1 mg/ml	20 mW	300	520	No	5×10^5	[20]
Pseudomonas aeruginosa	Gold nanorod	68 × 18	36 pM	80 mW	600	785	anti-PA3 antibody	1×10^8	[21]
Salmonella typhimurium	oval-shaped gold nanoparticle	20	-	40 mW	600	670	anti-salmonella antibody	5×10^3	[22]
Salmonella DT104	magnetic core– popcorn-shaped gold shell	20	-	2 W/cm^2	600	670	M3038 antibody	2.4×10^5	[23]

*Note: An anaerobic *Porphyromonas gingivalis* bacteria was examined in this study. *E. coli*, *Corynebacterium pseudotuberculosis* (*C. pseudotuberculosis*), *Pseudomonas aeruginosa* (*P. aeruginosa*), *Salmonella typhimurium* (*S. typhimurium*), and *Salmonella* DT104 are facultative anaerobic bacteria.

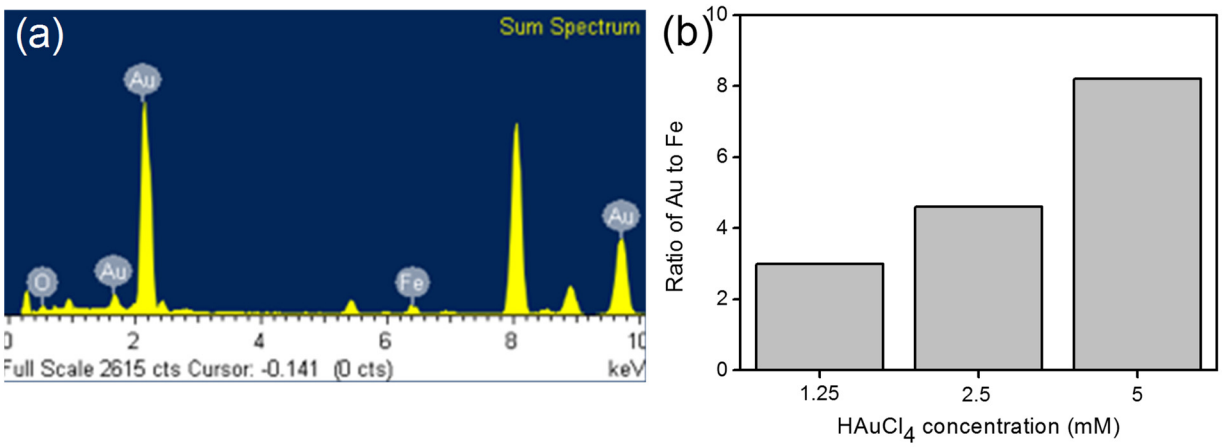

Figure S1. (a) EDX analysis of Fe_3O_4@Au nanohybrids with 5 mM of a $HAuCl_4$ solution and (b) AAS measurements of Fe_3O_4@Au nanohybrids with 1.25, 2.5, and 5 mM of $HAuCl_4$ solutions.

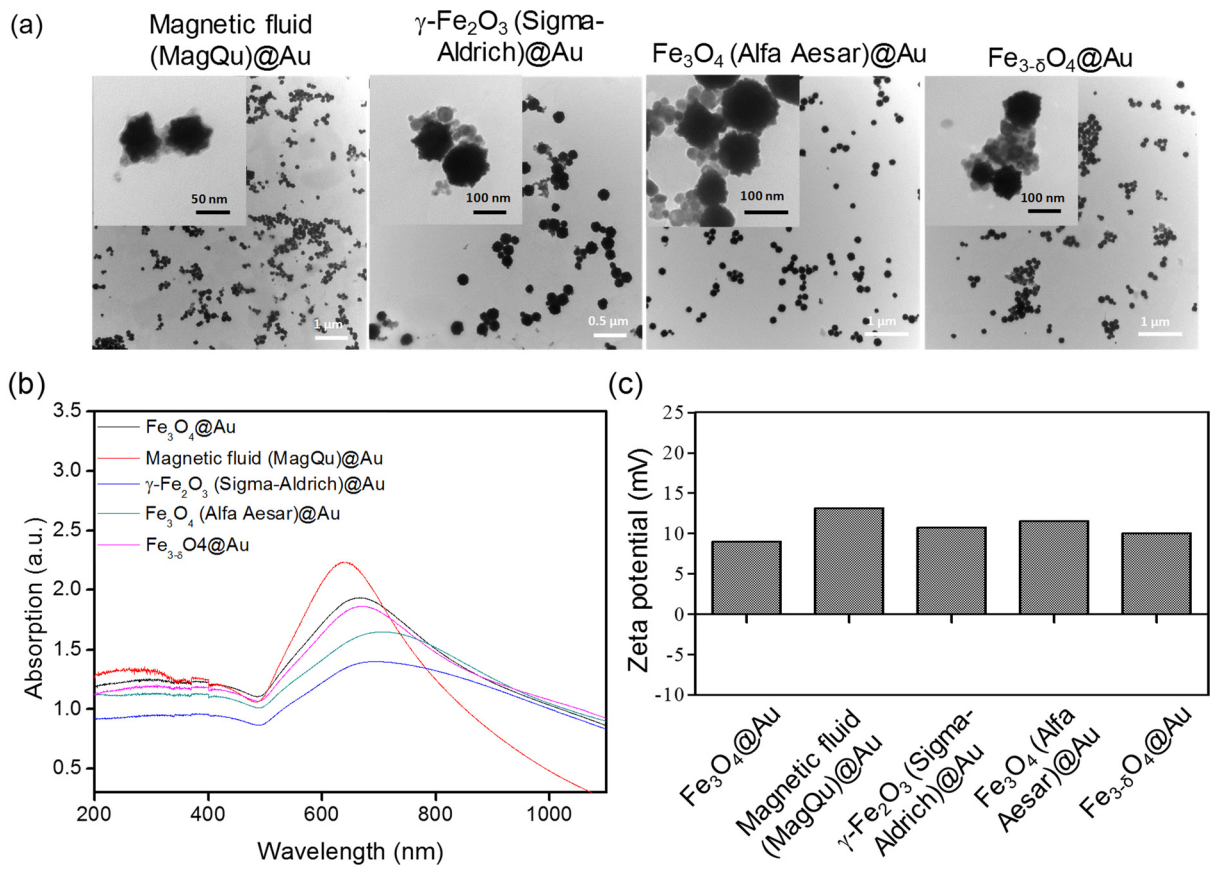

Figure S2. (a) TEM images, (b) UV-visible spectra, and (c) zeta potential of Fe_3O_4@Au nanohybrids by using magnetic fluid-carboxyl (MagQu, MF-COO-0060), iron(III) oxide Fe_2O_3 (Sigma-Aldrich, 544884), iron(II,III) oxide Fe_3O_4 (Alfa Aesar, 44665), and poly(styrene-alt-maleic acid) (PSMA) coated $Fe_{3-\delta}O_4$ nanoparticles[24] as starting materials for a subsequent reaction with 5 mM of $HAuCl_4$ solutions by the same procedure.

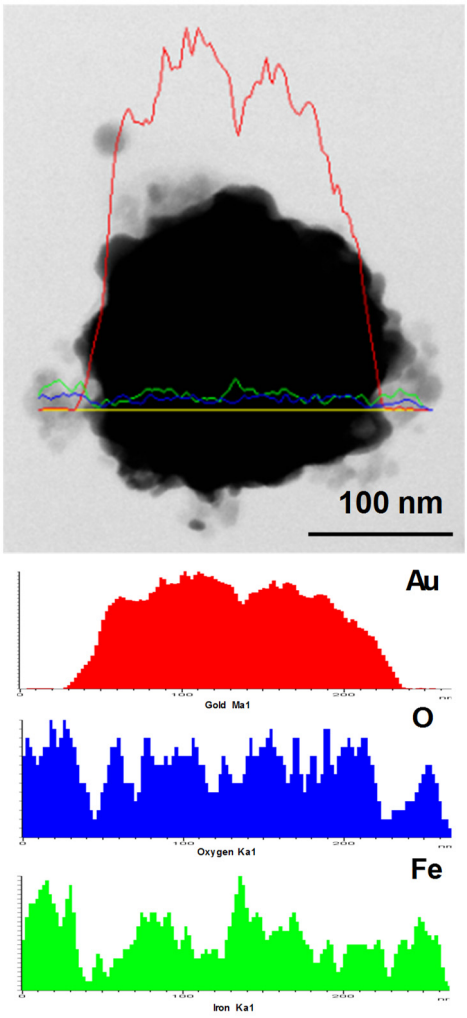

Figure S3. TEM line scan analysis of a single Fe_3O_4@Au nanohybrid along the yellow line in the image.

FT-IR spectroscopy was performed to characterize the polydopamine capping on the surface of the Fe_3O_4@Au nanohybrid, as shown in Figure S2. The high wavenumber region displayed peaks at 2848 cm^{-1}, 2917 cm^{-1} and 2959 cm^{-1} from aliphatic ν(C−H) stretching modes.[25] The broadened band between 1500 cm^{-1} and 1610 cm^{-1} was attributed to the peak overlap of the ν_{ring}(C=N) band at 1504 cm^{-1} and the ν_{ring}(C=C) band at 1576 cm^{-1} from the polydopamine structure. Two weak peaks at 1723 cm^{-1} and 1290 cm^{-1} were observed, corresponding to ν(C=O) vibrations due to the presence of quinone groups and C−O bonds, respectively.[25, 26] After the deposition of Au and polydopamine, a finite size effect for the specific Fe-O stretching vibrations of the Fe_3O_4 nanoparticle clusters was found based on the typical splitting peaks at 650 cm^{-1} and 573 cm^{-1} as well as the band at 438 cm^{-1}.[27] Based on these IR absorption peak assignments, the formation of the polydopamine composite after the reduction of $HAuCl_4$ and the preserved Fe_3O_4 crystal structure to form the Fe_3O_4@Au-polydopamine nanohybrid were confirmed.

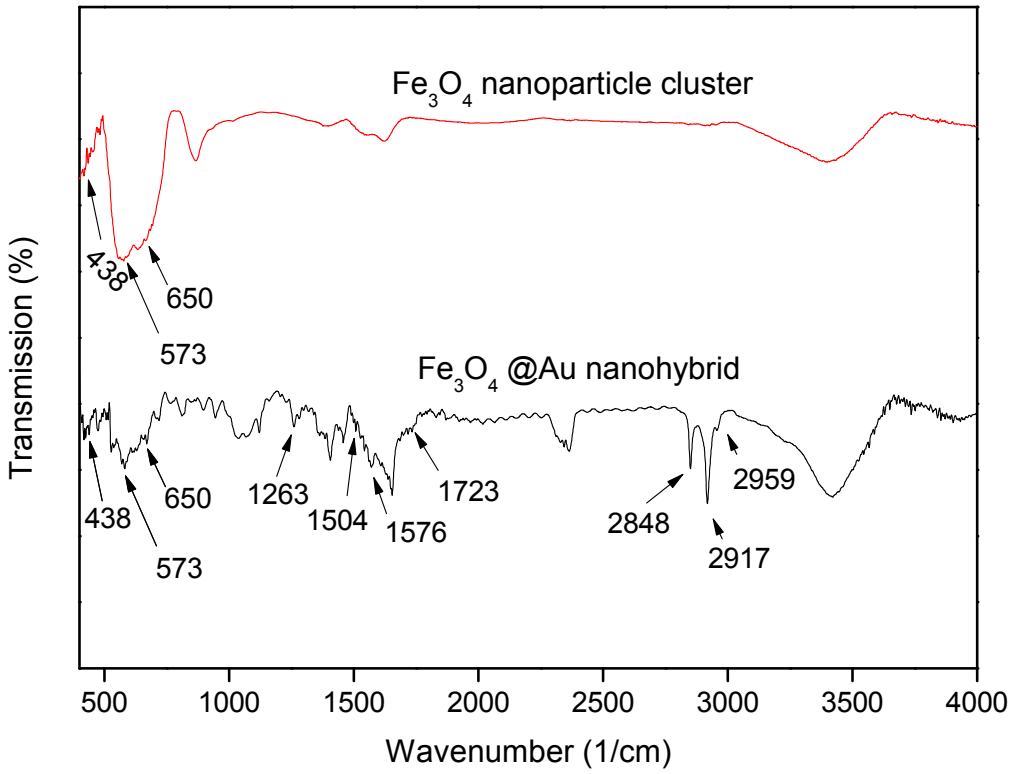

Figure S4. FT-IR spectra of the Fe_3O_4@Au nanohybrid and Fe_3O_4 nanoparticle clusters.

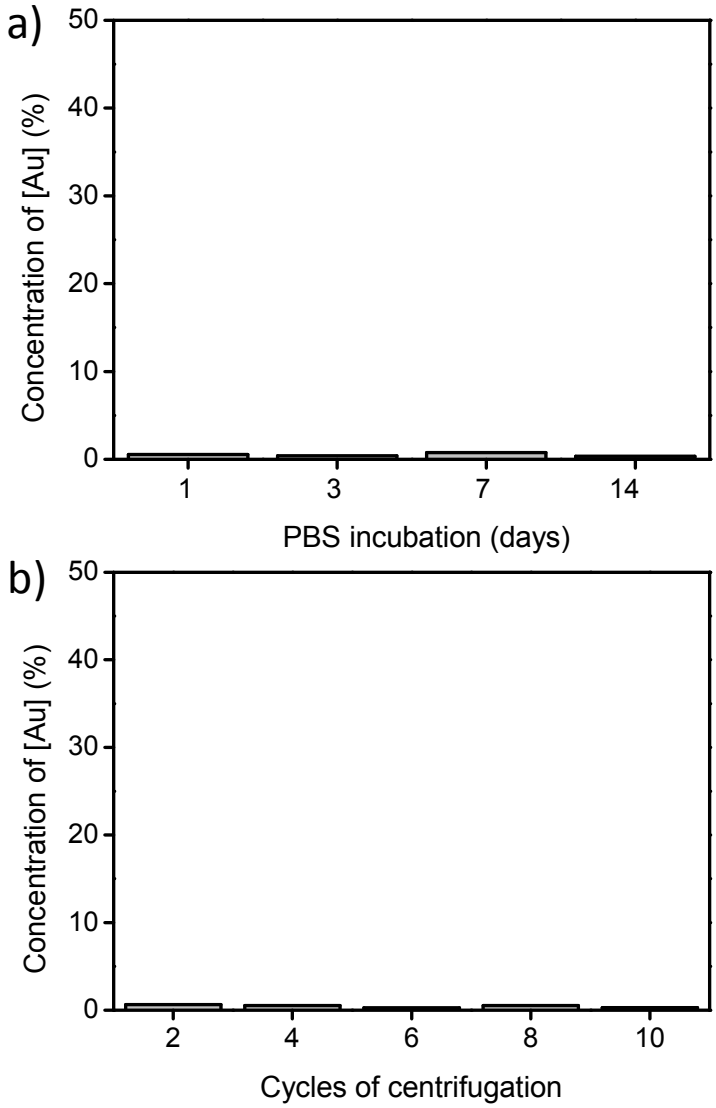

Figure S5. (a) AAS analysis of the supernatant solutions from the 50 $ppm_{[Fe]}$ (~1454 $ppm_{[Au]}$) Fe_3O_4@Au nanohybrids incubated in PBS solution for 1-14 days. The supernatant solution was collected after a centrifugation process at 2500 rpm (10 min). (b) AAS analysis of the supernatant solutions from the 50 $ppm_{[Fe]}$ (~1454 $ppm_{[Au]}$) Fe_3O_4@Au nanohybrids incubated in a PBS solution. The supernatant solutions were collected from different centrifugation steps after 13000 rpm for 10 min for each group.

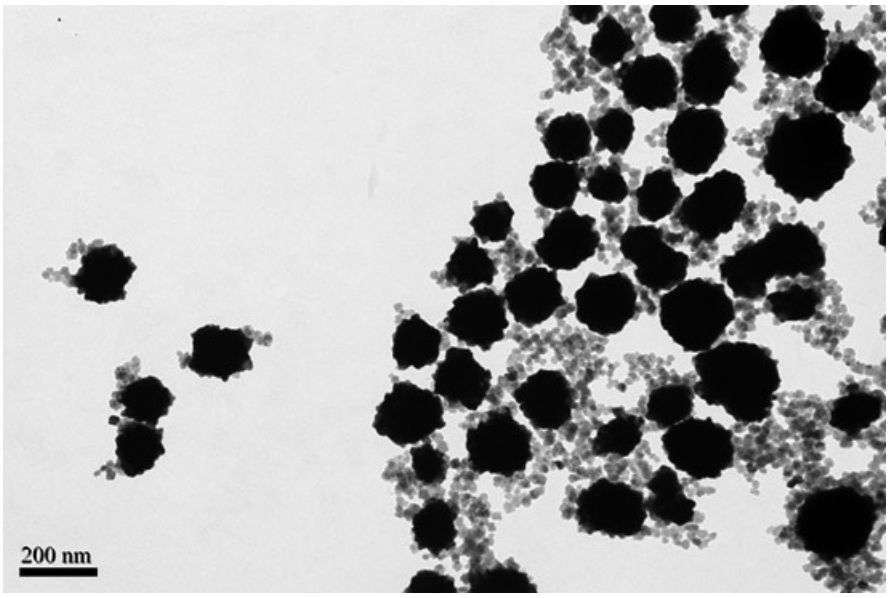

Figure S6. TEM images of the Fe_3O_4@Au nanohybrids collected from the precipitates at the 10^{th} centrifugation cycles. The centrifugation rate is 13000 rpm for 10 min for each group.

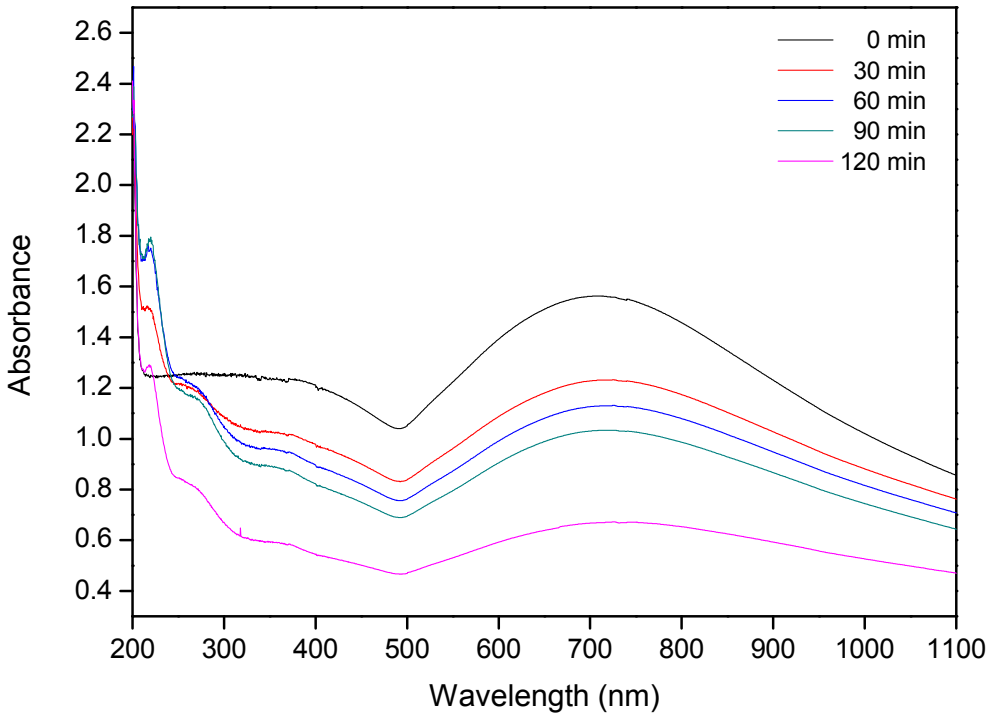

Figure S7. UV-vis absorption spectra of the Fe_3O_4@Au nanohybrid etched with 1.6 M HCl at different time points.

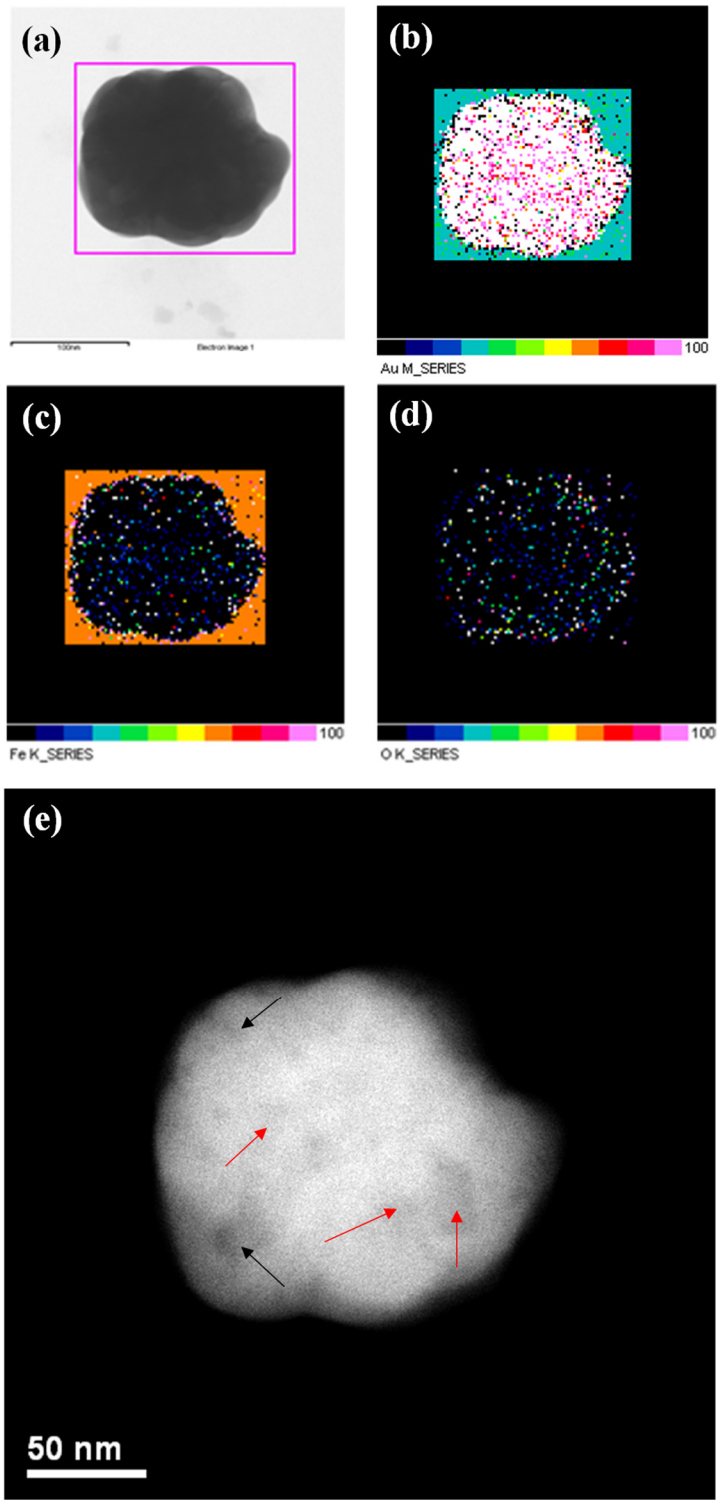

Figure S8. TEM image (a) and quantum map analyses of (b) Au, (c) Fe, and (d) O of the Fe_3O_4@Au nanohybrid after etching with 1.6 M HCl. (e) Corresponding HAADF-STEM image. The black and red arrows indicate the pore- and channel-like structures in the resulting Au particle.

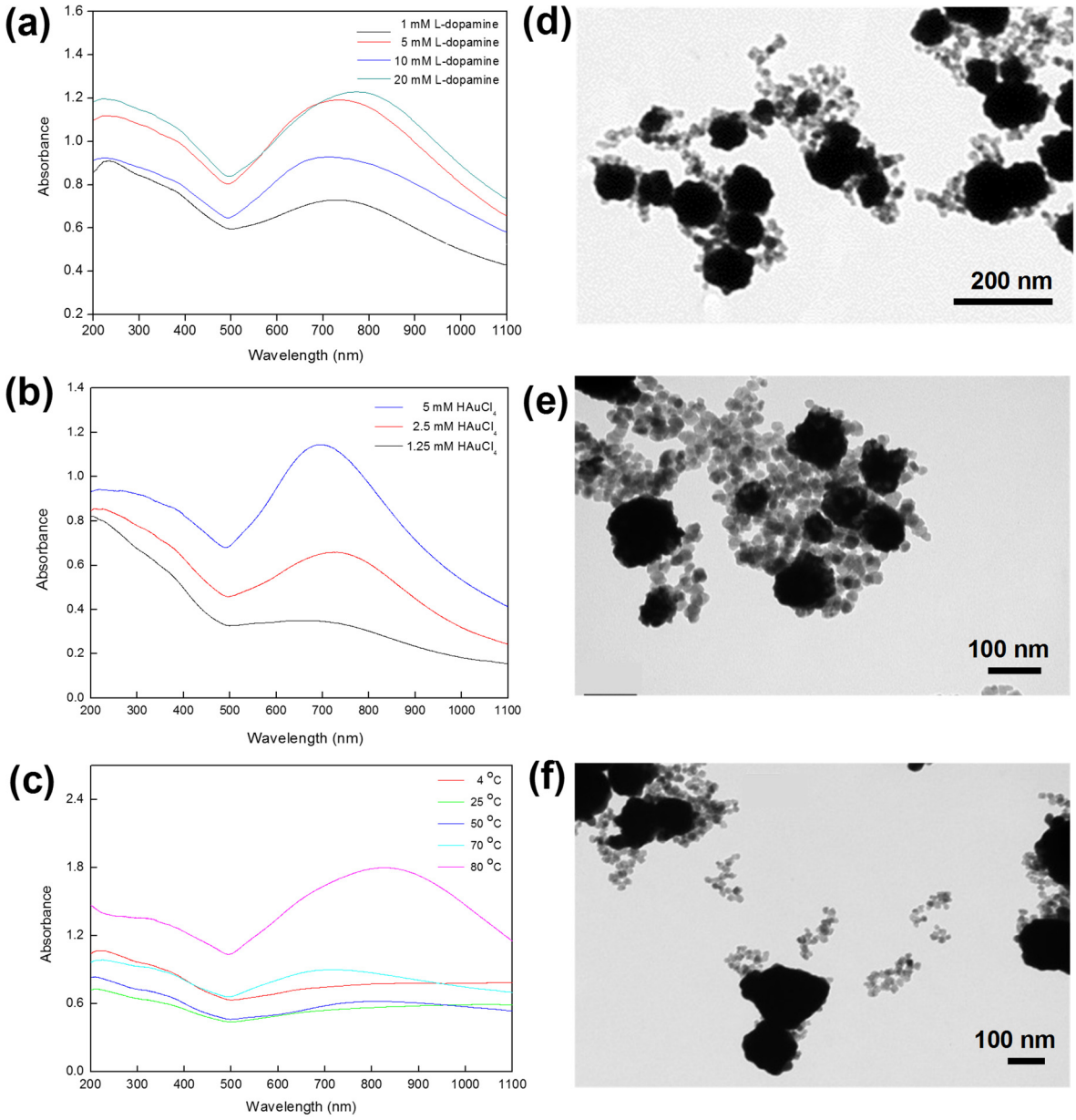

Figure S9. UV-visible measurements of the Fe_3O_4@Au nanohybrids prepared with various reaction parameters: (a) 5-20 mM L-dopamine, (b) 1.25-5 mM $HAuCl_4$, and (c) temperatures between 0 and 80 °C. TEM images of the Fe_3O_4@Au nanohybrids synthesized with 1 mM L-dopamine (d), 2.5 mM $HAuCl_4$ (e), and a reaction temperature of 4 °C (f).

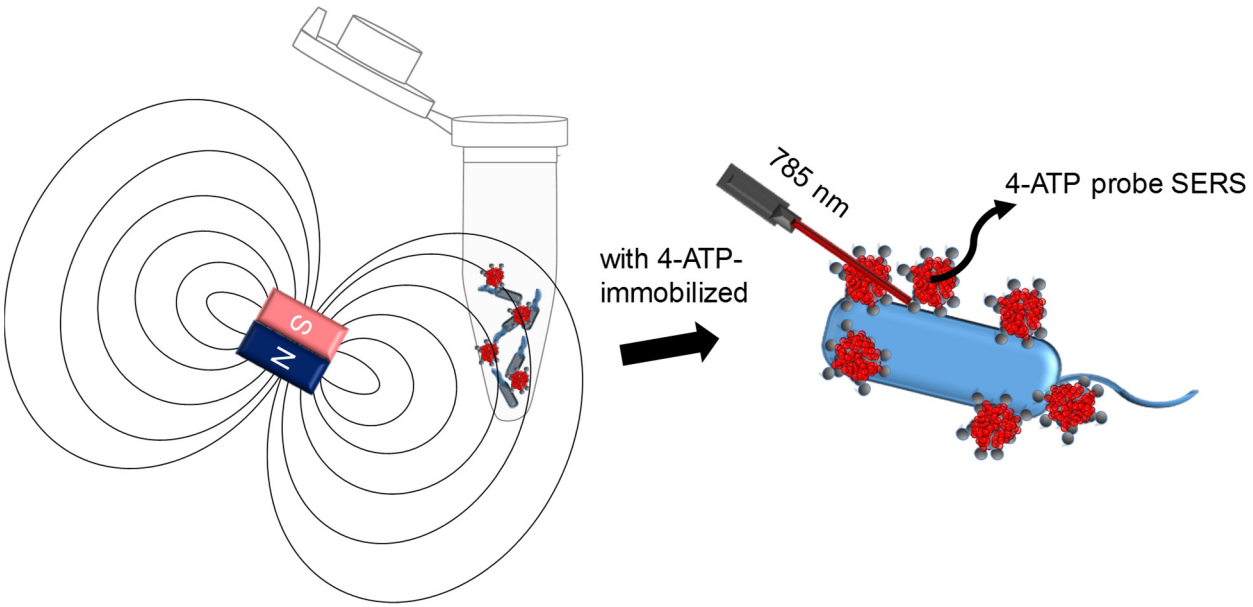

Figure S10. Scheme of 4-ATP probe-immobilized Fe_3O_4@Au nanohybrid-treated bacteria isolated with an external magnetic field followed by an SERS measurement.

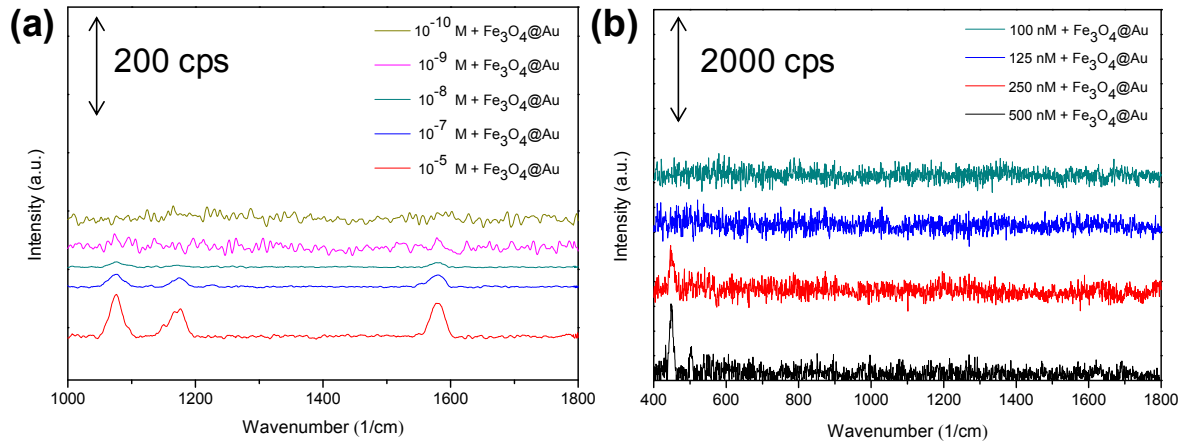

Figure S11. Sensitivity of the SERS sensing of (a) 4-ATP (10^{-3}-10^{-10} M) and (b) MB (10^{-3}-10^{-7} M) combined with the Fe_3O_4@Au nanohybrids.

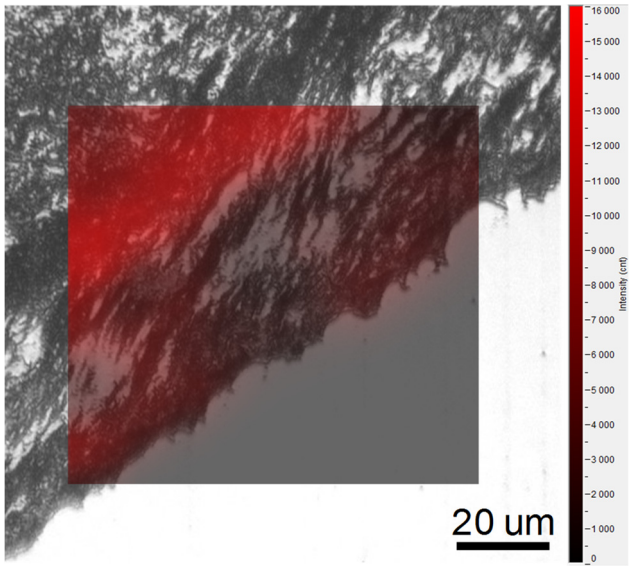

Figure S12. Raman mapping image (selected peak at 1592 cm^{-1}) merged with the bright image of the 4-ATP-coated Fe_3O_4@Au nanohybrid concentrated onto a Si wafer by a magnet.

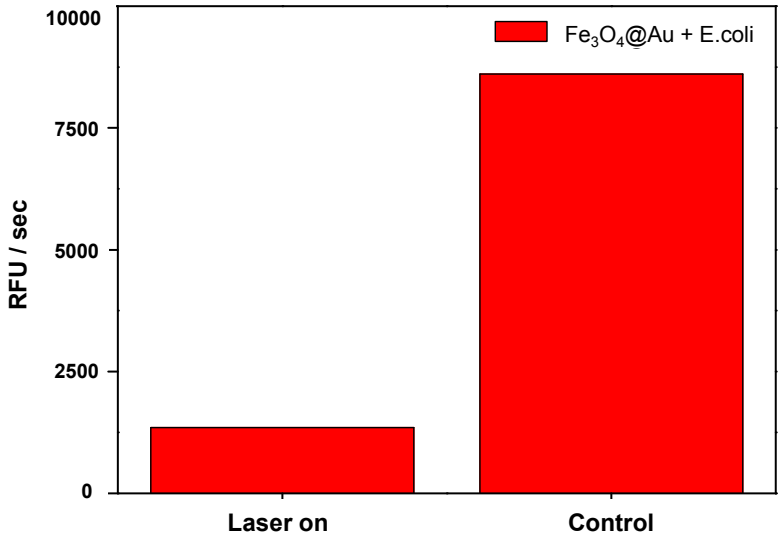

Figure S13. Cell viability of *E. coli* treated with the Fe_3O_4@Au nanohybrid and irradiated with an 808 nm laser. ATP level of *E. coli* presenting the cell viability as determined by the BacTiter-Glo^{TM} Microbial Cell Viability Assay.

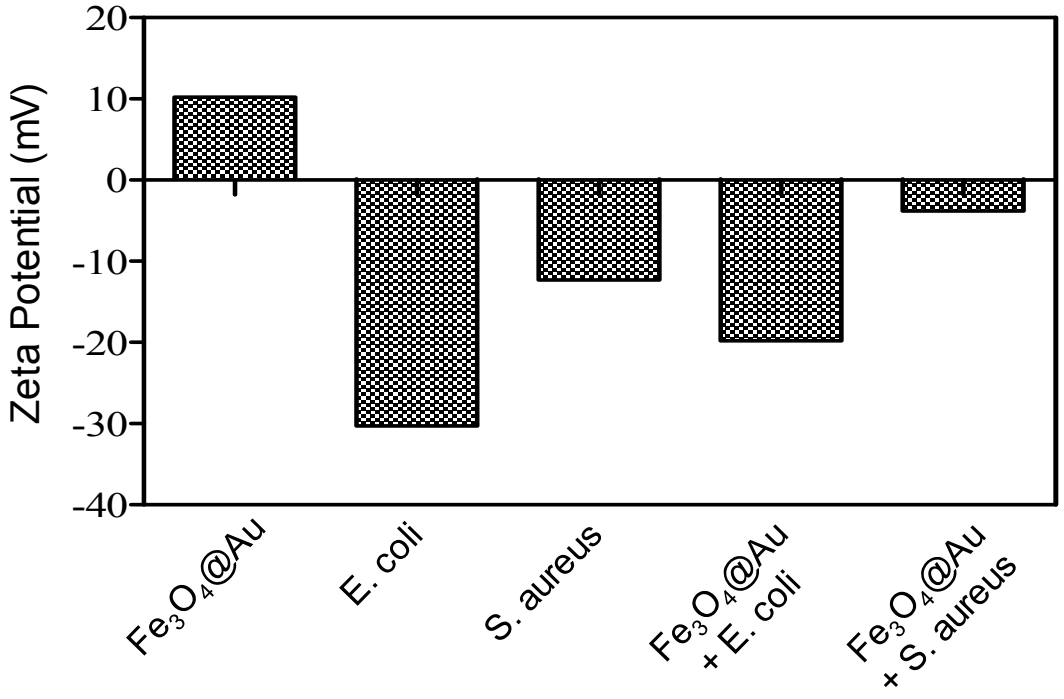

Figure S14. Zeta potential measurements of *E. coli* or *S. aureus* before and after incubation with the Fe_3O_4@Au nanohybrids.

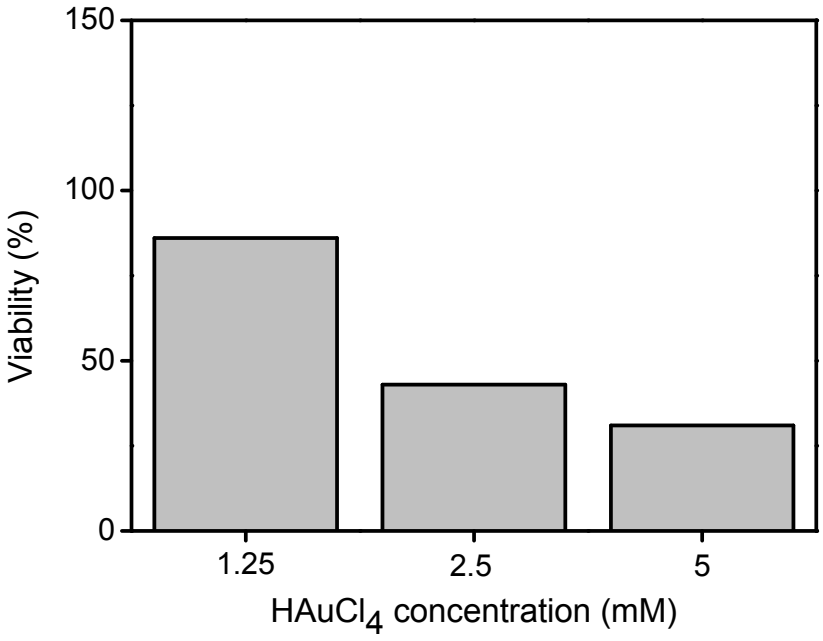

Figure S15. Bacterial viability of *E. coli* after treating with 25 $ppm_{[Fe]}$ (~727 $ppm_{[Au]}$) Fe_3O_4@Au nanohybrids synthesized from 1.25, 2.5, and 5 mM $HAuCl_4$ solutions and then irradiating with an 808 nm laser (1.25 W/cm^2) for 10 min.

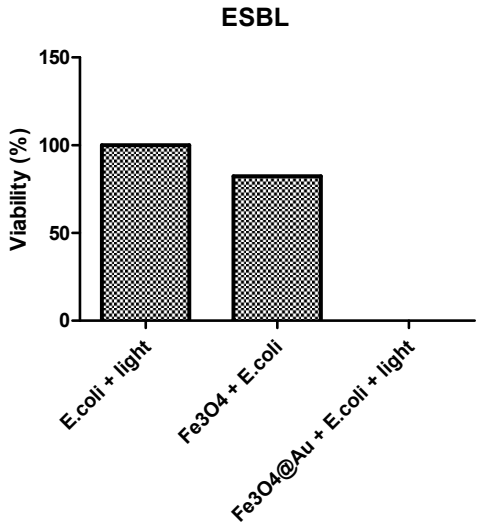

Figure S16. Cell viability of ESBL *E. coli* treated with the Fe_3O_4@Au nanohybrids and irradiated with an 808 nm laser.

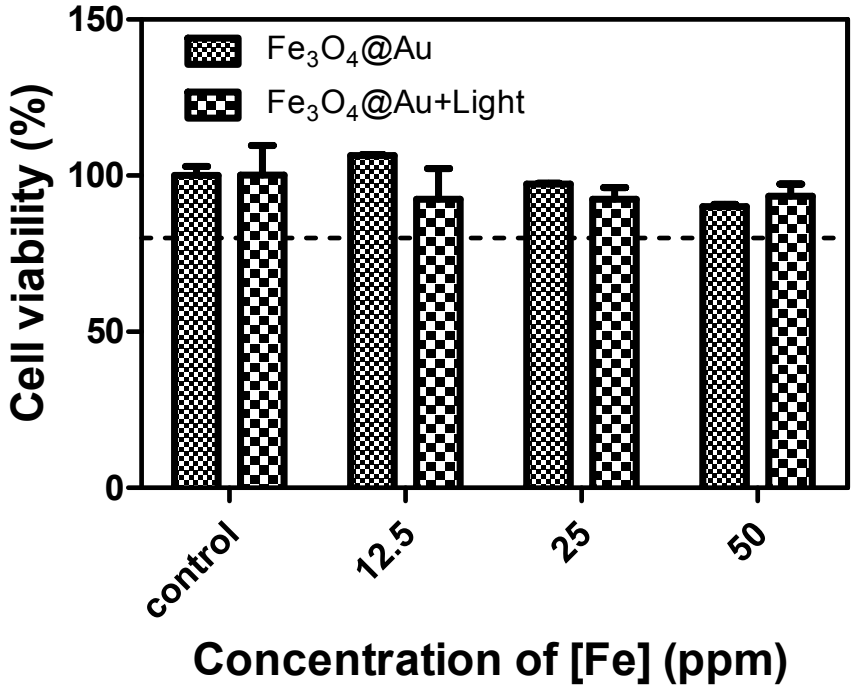

Figure S17. Cytotoxicity of Fe_3O_4@Au nanohybrids on normal cells. NIH/3T3 (mouse normal embryo fibroblast) cells were incubated with Fe_3O_4@Au nanohybrids for 24 h or incubated with Fe_3O_4@Au nanohybrids for 3 h, followed by PBS washing and irradiation with 808 nm light (1.25 W/cm^2) for 10 min.

Reference

1. C. C. Huang, P. Y. Chang, C. L. Liu, J. P. Xu, S. P. Wu and W. C. Kuo, *Nanoscale*, 2015, **7**, 12689-12697.
2. L. León Félix, J. A. H. Coaquira, M. A. R. Martínez, G. F. Goya, J. Mantilla, M. H. Sousa, L. d. l. S. Valladares, C. H. W. Barnes and P. C. Morais, *Sci Rep*, 2017, **7**, 41732.
3. E. Fantechi, A. G. Roca, B. Sepúlveda, P. Torruella, S. Estradé, F. Peiró, E. Coy, S. Jurga, N. G. Bastús, J. Nogués and V. Puntes, *Chem Mater*, 2017, **29**, 4022-4035.
4. V. Victor, M. Laura, M. Eva, M. Nieves, H. Pilar, H. Antonio and C. Patricia, *J Phys D: Appl Phys*, 2015, **48**, 035502.
5. H. Yu, M. Chen, P. M. Rice, S. X. Wang, R. L. White and S. Sun, *Nano Lett*, 2005, **5**, 379-382.
6. C. Wang, J. Qian, K. Wang, X. Yang, Q. Liu, N. Hao, C. Wang, X. Dong and X. Huang, *Biosens Bioelectron*, 2016, **77**, 1183-1191.
7. P. G. Rudakovskaya, E. K. Beloglazkina, A. G. Majouga and N. V. Zyk, *Mendeleev Commun*, 2010, **20**, 158-160.
8. Z. Xu, Y. Hou and S. Sun, *JACS*, 2007, **129**, 8698-8699.
9. W. Dong, Y. Li, D. Niu, Z. Ma, J. Gu, Y. Chen, W. Zhao, X. Liu, C. Liu and J. Shi, *Adv Mater*, 2011, **23**, 5392-5397.
10. H. Y. Xie, R. Zhen, B. Wang, Y. J. Feng, P. Chen and J. Hao, *J Phys Chem C*, 2010, **114**, 4825-4830.
11. J. Huang, M. Guo, H. Ke, C. Zong, B. Ren, G. Liu, H. Shen, Y. Ma, X. Wang, H. Zhang, Z. Deng, H. Chen and Z. Zhang, *Adv Mater*, 2015, **27**, 5049-5056.
12. W. C. Huang, P. J. Tsai and Y. C. Chen, *Small*, 2009, **5**, 51-56.
13. Q. Ding, H. Zhou, H. Zhang, Y. Zhang, G. Wang and H. Zhao, *Journal of Materials Chemistry Journal of materials chemistry A*, 2016, **4**, 8866-8874.
14. C. Wang, J. Wang, M. Li, X. Qu, K. Zhang, Z. Rong, R. Xiao and S. Wang, *Analyst*, 2016, **141**, 6226-6238.
15. B. Hu, L. P. Zhang, X. W. Chen and J. H. Wang, *Nanoscale*, 2013, **5**, 246-252.
16. W. C. Huang, P. J. Tsai and Y. C. Chen, *Nanomedicine*, 2007, **2**, 777-787.
17. M. C. Wu, A. R. Deokar, J. H. Liao, P. Y. Shih and Y. C. Ling, *ACS Nano*, 2013, **7**, 1281-1290.
18. L. Mocan, C. Matea, F. A. Tabaran, O. Mosteanu, T. Pop, C. Puia, L. Agoston-Coldea, D. Gonciar, E. Kalman, G. Zaharie, C. Iancu and T. Mocan, *Sci Rep*, 2016, **6**, 39466.
19. Z. Zhao, R. Yan, X. Yi, J. Li, J. Rao, Z. Guo, Y. Yang, W. Li, Y.-Q. Li and C. Chen, *ACS Nano*, 2017, **11**, 4428-4438.
20. M. M. Mohamed, S. A. Fouad, H. A. Elshoky, G. M. Mohammed and T. A. Salaheldin, *Int J Vet Sci Med*, 2017, **5**, 23-29.
21. R. S. Norman, J. W. Stone, A. Gole, C. J. Murphy and T. L. Sabo-Attwood, *Nano Lett*, 2008,

8, 302-306.

22. S. Wang, A. K. Singh, D. Senapati, A. Neely, H. Yu and P. C. Ray, *Chem Eur J*, 2010, **16**, 5600-5606.
23. Z. Fan, D. Senapati, S. A. Khan, A. K. Singh, A. Hamme, B. Yust, D. Sardar and P. C. Ray, *Chem Eur J*, 2013, **19**, 2839-2847.
24. C. C. Huang, K. Y. Chuang, C. P. Chou, M. T. Wu, H. S. Sheu, D. B. Shieh, C. Y. Tsai, C. H. Su, H. Y. Lei and C. S. Yeh, *J Mater Chem*, 2011, **21**, 7472-7479.
25. R. A. Zangmeister, T. A. Morris and M. J. Tarlov, *Langmuir*, 2013, **29**, 8619-8628.
26. H. Luoa, C. Gua, W. Zhengb, F. Daia, X. Wanga and Z. Zheng, *The Royal Society of Chemistry*, 2015, **5**.
27. M. Ma, Y. Zhang, W. Yu, H. Y. Shen, H. Q. Zhang and N. Gu, *Colloids Surf A Physicochem Eng Asp*, 2003, **212**, 219-226.